Use of Landsat data to track historical water quality changes in Florida Keys marine environments

Article *in* Remote Sensing of Environment · January 2014

DOI: 10.1016/j.rse.2013.09.020

Remote Sensing of Environment 140 (2014) 485–496

Contents lists available at ScienceDirect

Remote Sensing of Environment

journal homepage: www.elsevier.com/locate/rse

Use of Landsat data to track historical water quality changes in Florida Keys marine environments

Brian B. Barnes [a,*], Chuanmin Hu [a], Kara L. Holekamp [b,c], Slawomir Blonski [b,d], Bruce A. Spiering [e], David Palandro [f], Brian Lapointe [g]

[a] College of Marine Science, University of South Florida, 140 7th Ave South, St. Petersburg, FL 33701, USA
[b] Science Systems & Applications, Inc., Stennis Space Center, MS, USA
[c] Innovative Imaging & Research, Stennis Space Center, MS, USA
[d] Earth System Science Interdisciplinary Center, University of Maryland, College Park, MD, USA
[e] NASA Applied Science & Technology Project Office, Stennis Space Center, MS, USA
[f] ExxonMobil Upstream Research Company, Houston, TX, USA
[g] Harbor Branch Oceanographic Institute, Florida Atlantic University, Fort Pierce, FL, USA

ARTICLE INFO

Article history:
Received 6 June 2013
Received in revised form 18 September 2013
Accepted 19 September 2013
Available online xxxx

Keywords:
Water quality
Remote sensing
Atmospheric correction
Seagrass

ABSTRACT

Satellite remote sensing has shown the advantage of water quality assessment at synoptic scales in coastal regions, yet modern sensors such as SeaWiFS or MODIS did not start until the late 1990s. For non-interrupted observations, only the Landsat series have the potential to detect major water quality events since the 1980s. However, such ability is hindered by the unknown data quality or consistency through time. Here, using the Florida Keys as a case study, we demonstrate an approach to identify historical water quality events through improved atmospheric correction of Landsat data and cross-validation with concurrent MODIS data. After aggregation of the Landsat-5 Thematic Mapper (TM) 30-m pixels to 240-m pixels (to increase the signal-to-noise ratio), a MODIS-like atmospheric correction approach using the Landsat shortwave-infrared (SWIR) bands was developed and applied to the entire Landsat-5 TM data series between 1985 and 2010. Remote sensing reflectance (R_{RS}) anomalies from Landsat (2 standard deviations from a pixel-specific monthly climatology) were found to detect MODIS R_{RS} anomalies with over 90% accuracy for all three bands for the same period of 2002–2010. Extending this analysis for the entire Landsat-5 time-series revealed R_{RS} anomaly events in the 1980s and 1990s, some of which are corroborated by known ecosystem changes due in part to changes in local freshwater flow. Indeed, TM R_{RS} anomalies were shown to be useful in detecting shifts in seagrass density, turbidity increases, black water events, and phytoplankton blooms. These findings have large implications for ongoing and future water quality assessment in the Florida Keys as well as in many other coastal regions.

1. Introduction

One of the challenges in remote sensing is placing measurements in the context of events before and after the life of an instrument. Several studies have compared the data of multiple satellite instruments in efforts to extend the time series of remotely sensed data (e.g., Maritorena & Siegel, 2005), occasionally finding significant disagreement in both time and space (e.g., Franz, 2003; Kwiatkowska, 2003). Even so, temporal gaps exist during which little to no satellite data are available. For ocean color remote sensing, which has been shown to be particularly useful in assessing optical water quality of coastal waters, such a data gap exists after the Coastal Zone Color Scanner (CZCS) stopped functioning in early 1986 and before the Sea-viewing Wide Field-of-view Sensor (SeaWiFS) was launched in late 1997.

Throughout this gap, however, satellites dedicated to land study continued to collect multi-spectral radiance data over coastal waters. The Landsat program began in 1972, and through eight satellites has maintained a nearly continuous record of satellite data for land and adjacent coastal waters. Landsat-5 (1984–2011) housed a Thematic Mapper (TM) sensor, which measured radiance with 30 m spatial resolution for 6 bands (three visible, three infrared), and thermal infrared (TIR) radiation at 120 m resolution. Each Landsat satellite has a polar earth orbit, crossing the equator at approximately 10:00 am local time with 185 km Earth-viewing swath width. As a result, repeat sampling for a particular location occurs at 16-day intervals. Although its primary purpose is for use over land, Landsat data collected over coastal and inland waters have been used with varying success to detect features including eddies (Ahlnäs, Royer, & George, 1987), phytoplankton blooms (Ekstrand, 1992), freshwater discharges (Lapointe, Matzie, & Clark, 1993), floating algae (Hu, 2009), cyanobacteria blooms (Vincent et al., 2004), water quality (Dekker & Peters, 1993; Giardino, Pepe, Brivio, Ghezzi, & Zilioli, 2001; Olmanson, Bauer, & Brezonik, 2008;

* Corresponding author. Tel.: +1 727 553 3952.
E-mail address: bbarnes4@mail.usf.edu (B.B. Barnes).

0034-4257/$ – see front matter © 2013 Elsevier Inc. All rights reserved.
http://dx.doi.org/10.1016/j.rse.2013.09.020

Wang, Xia, Fu, & Sheng, 2004), sea surface temperatures (Thomas, Byrne, & Weatherbee, 2002), and coral community changes (Palandro, Andrefouet, Muller-Karger, & Dustan, 2001; Palandro et al., 2008), among others.

Since 2000 and 2002, respectively, the Moderate Resolution Imaging Spectroradiometers (MODIS) aboard the U.S. National Aeronautics and Space Administration (NASA)'s polar orbiting satellites Terra and Aqua (MODIST and MODISA) have provided near-daily measurements of radiance over the world's oceans after the CZCS (1978–1986) and SeaWiFS (1997–2010) eras. Most MODIS bands cover a spectral bandwidth of 10–20 nm with the spatial resolution of 250 m–1000 m. Aqua ascends across the equator at approximately 1:30 pm local time for daytime passes with a swath width of 2330 km, while Terra descends across the equator at 10:30 am local time with the same swath width.

Despite significant differences in the spectral and spatial resolutions as well as in the signal-to-noise ratios (SNR) between MODIS and TM (Hu et al., 2012), similarities in their spectral band positions indicate the potential for filling the 1986–1997 historical data gap using Landsat TM. The satellites housing these instruments all orbit at an altitude of 705 km with nearly identical inclination (98.20° for Landsat 5, 98.14° for Aqua). The TM visible band centers (485, 560, and 660 nm for bands 1, 2, and 3) roughly correspond to those of MODIS bands 10, 4, and 13 (centers at 488, 555, and 667 nm; Fig. 1). For simplicity, these corresponding bands for both sensors are termed 'blue', 'green' and 'red,' respectively. Despite these similar band centers, there are large differences in spectral resolution between these TM (~70 nm) and MODISA bands (10–20 nm).

The narrow swath width of the Landsat TM measurements (185 km) every 16 days and the much wider swath of MODIS measurements (2330 km) every 1–2 days mean that nearly every Landsat image has a corresponding MODIS image on the same day. Although Terra coincides more closely with Landsat overpass times, significant residual errors due to striping and scan mirror damage limit MODIST data applicability for ocean color research (Franz, Kwiatkowska, Meister, & McClain, 2008). However, MODISA has provided quality data since 2002. It is therefore desirable to validate the quality and accuracy of Landsat TM data using concurrent MODISA data so that water quality data derived from MODISA can be extended to the 1980s.

Our approach to fill the 1986–1997 satellite ocean color gap through cross-validation of TM and MODIS data was motivated by several factors. First, MODIS ocean color bands were designed for research of water targets, while TM was intended for land assessment. As a result, achieving MODIS-quality data from TM imagery (rather than simply using TM data) is preferable for ocean color research. Second, cross-validation of TM with MODISA data will provide high-frequency (albeit low resolution) continuation and supplementation of the Landsat dataset. At the time of this research, Landsat 5 was defunct, and Landsat 7 suffered a scan line corrector (SLC) failure. Although compromised Landsat 7 images can be used to measure water parameters (see Olmanson et al., 2008), the SLC failure effectively reduces repeat sampling frequency. Landsat 8 includes an ocean color band in the blue, but it was only launched recently and its data were not available until 2013. MODIS data could serve as a bridge between these three sensors, and the regular overlap between MODIS and Landsat allows opportunities to assess instrument drift. This is in contrast to the cross-calibration between Landsat sensors, which is completed over a very short time window during which the instruments are placed in parallel orbits (see Teillet et al., 2001). Finally, the high repeat sampling frequency of MODIS sensors allows for creation of monthly or seasonal climatologies, which can be used to compare water quality events to the average condition over the last decade. Alone, the Landsat dataset lacks capacity to place ephemeral water quality features in the context of climatological norms due to the 16 day repeat sampling frequency. Proper cross-validation of these two sensors, however, would allow such assessment of TM detected events, which would significantly enhance our ability to study historical water quality events in coastal waters.

Extending MODIS observations in the 2000s to the 1980s and 1990s using Landsat TM, however, is technically challenging because of the sensors' differences in 1) band width and band positions; 2) radiometric calibration; 3) solar and viewing geometry; 4) SNR; and 5) overpass time. Although one may assume that the difference in their overpass time (2–3 h) may not result in significant changes in either the atmospheric or the water properties, and that the lower SNR in Landsat TM data may be increased by pixel binning, the first three issues must be adequately addressed in order to use Landsat TM data in a similar fashion as with MODISA. Thus, in this study, an approach was developed to overcome the first three obstacles in order to make Landsat data comparable to MODIS and to subsequently assess historical water quality events. For demonstration of this application to use long-term Landsat TM data to study changes of the coastal ocean, we selected a delicate Florida Keys ecosystem that encompasses world renowned coral reefs, beaches, and seagrasses. Such analysis would provide information on the effects of Everglades water management and restoration practices on the water quality of downstream systems. Further, the ability to locate water quality events (in space and time) could provide a record of previous environmental stress and hint at resilience to future stressors for enduring organisms. Specifically, the study had the following objectives:

1) To develop a practical method to construct a long-term time series of atmospherically corrected Landsat TM data, validated for ocean color research;
2) To apply the dataset to identify historical water quality events in the Florida Keys ecosystem.

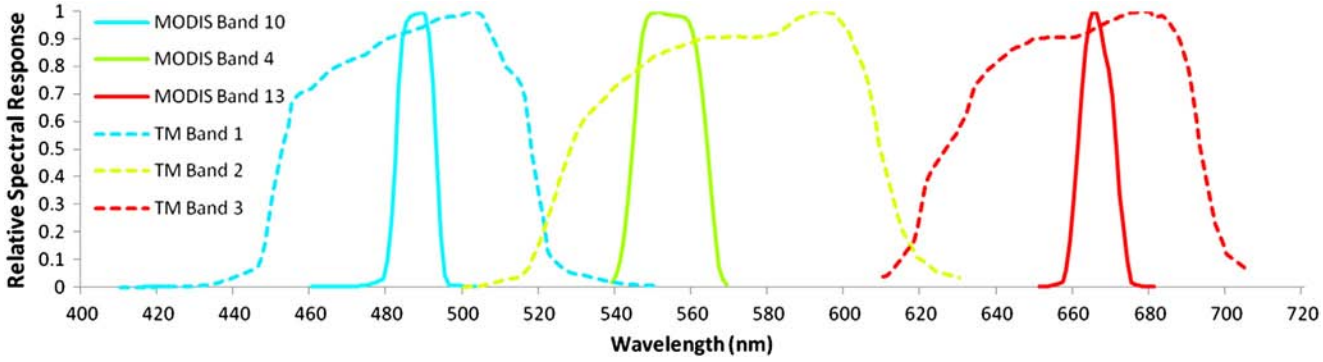

Fig. 1. Relative spectral response functions for Landsat TM bands (dashed) and MODISA bands (solid). Line color represents center wavelength for each band. (For interpretation of the references to color in this figure legend, the reader is referred to the web version of this article.)

2. Case study area — Florida Keys and surrounding waters

The Florida Keys is a 120 mile long archipelago of limestone islands located south of the Florida peninsula. Home to over 73,000 residents (US Census Bureau, 2011), these islands are a popular tourist destination, with approximately 2.5 million visitors annually generating nearly 1.2 billion dollars for the region (Causey, 2002). The waters surrounding the Florida Keys house a variety of shallow marine environments, including seagrass beds and coral reefs. Protection of these marine resources prompted the United States Congress in 1990 to create the Florida Keys National Marine Sanctuary (FKNMS), a 9600 km^2 marine protected area enveloping the Florida Keys.

Upstream of the Florida Keys marine ecosystems are the Florida Everglades, a subtropical wetland environment covering much of south Florida. Portions of the Everglades are also designated as protected areas, including the Big Cypress National Preserve and the Everglades National Park. The Shark and Caloosahatchee Rivers are major outflows of the Florida Everglades, leading into the Florida Keys region via Florida Bay and the Southwest Florida Bight (Fig. 2). Beginning in the early 1980s, due to concerns of hypersalinity affecting the marine ecosystems in Florida Bay and eutrophication of Lake Okeechobee, the Everglades Agricultural Area ceased pumping water runoff into Lake Okeechobee, instead diverting it to the riverine outflows. Although little data exist documenting the water quality of Florida Bay prior to the late 1980s, extremely clear water conditions were observed to be the norm (Fourqurean & Robblee, 1999; Stumpf, Frayer, Durako, & Brock, 1999). In the years since, the Florida Bay ecosystem has experienced large changes in water quality, concurrent with massive die-offs of seagrasses (Fourqurean & Robblee, 1999; Lapointe, Barile, & Matzie, 2004; Lapointe, Matzie, & Barile, 2002; Robblee et al., 1991; Stumpf et al., 1999). Much research suggests that increasing nutrient concentrations were responsible for seagrass declines in the Florida Keys region through epiphytization (Lapointe & Barile, 2004; Lapointe & Clark, 1992), competition with macroalgal species (Lapointe et al., 2002) or shading by phytoplankton blooms and increased turbidity (Lapointe & Clark, 1992; Lapointe et al., 2004; Phlips, TC, L., & S, B., 1995). Although hypersalinity has also been proposed as a mechanism for seagrass decline (Robblee et al., 1991; Zieman, Fourqurean, & Frankovich, 1999), the conclusion that hypersalinity caused the Florida Bay seagrass declines is questionable (National Research Council, 2002).

Smith and Pitts (2002) found net water flow from Florida Bay to the Atlantic Ocean side of the Florida Keys via tidal passes between the islands. As such, the water conditions in Florida Bay can impact the Florida Reef Tract (FRT), a string of bank reef environments south and east of the Florida Keys. Coral cover in the FRT has been in decline for several decades (Dustan, 2003; Palandro et al., 2001, 2008; Porter et al., 2002) due in part to changes in water quality. Indeed, Lapointe et al. (2004) found anthropogenic enrichment of nitrogen is a key causative factor for macroalgal blooms on the FRT and subsequent declines in coral cover. Other factors which have been implicated in coral declines include overfishing (Ault, Bohnsack, Smith, & Luo, 2005; Miller & Hay, 1998), macroalgal blooms resulting from urchin mass mortalities (Lessios, Robertson, & Cubit, 1984), African dust (Garrison et al., 2003; Shinn et al., 2000), vessel groundings (Ebersole, 2001), coral diseases (Porter et al., 2001), extreme temperature events (Jaap, 1985; Lirman et al., 2011; Warner, Fitt, & Schmidt, 1999), and water quality events (Hu, Muller-Kager, Vargo, Neely, & Johns, 2004; Hu et al., 2003; Zhao et al., 2013).

For this study, four discrete locations were selected as representative examples of Florida Bay (A; 24.91°N, 81.08°W), Upper Keys (B; 24.97°N, 81.5°W) Middle Keys (C; 24.65°N, 81.14°W) and Lower Keys (D; 24.55°N, 81.56°W) waters (Fig. 2). Also, two transects were drawn

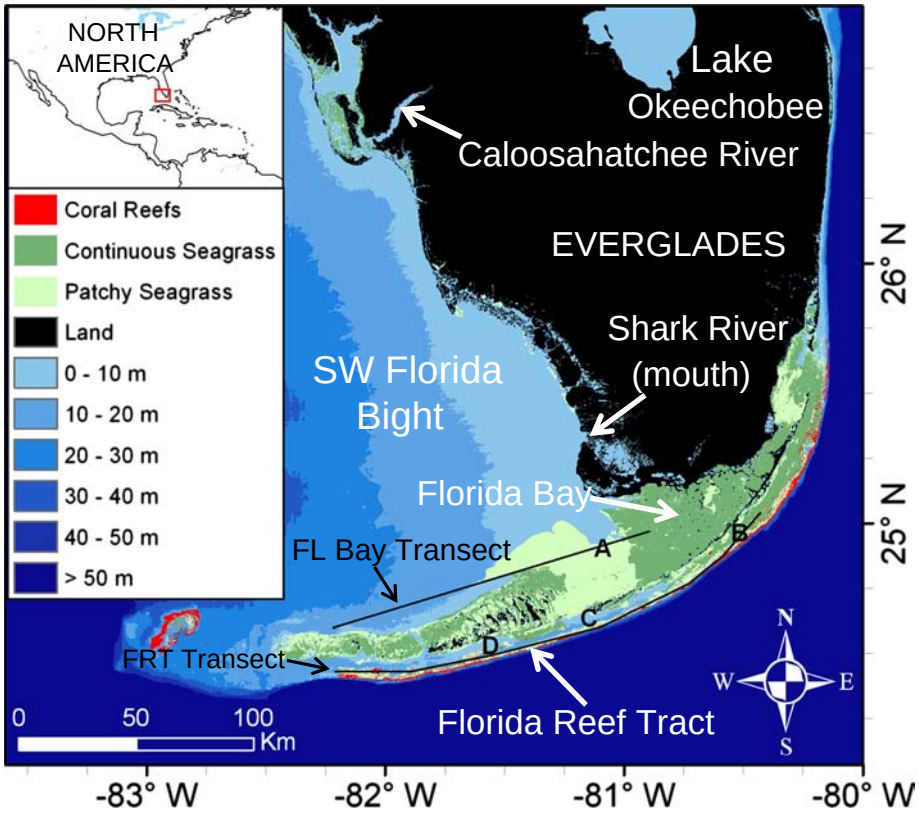

Fig. 2. Map showing the study region including bathymetry from National Geophysical Data Center coastal relief models. Seagrass environments (patchy and continuous, compiled using Florida Fish and Wildlife Research Institute data from 1987 to 2008) are shown in green, coral reefs (patch and bank reefs) in red, land in black, and depth range in shades of blue. A, B, C, and D are locations used for time series analysis.

to visualize spatiotemporal patterns. Within Florida Bay/SW Florida Bight, the transect was selected to maximize data coverage and span a variety of environments including seagrass and sponge beds. The second transect, south of the Florida Keys, captures patch and bank coral reef environments in addition to seagrass beds.

3. Methods — Data source and processing

Although CZCS provided satellite ocean color over the region between 1978 and 1986, it is unknown whether CZCS data could provide consistent data with modern sensors such as MODISA. In contrast, the long-term measurements of Landsat 5 TM (1984–2011) provide an opportunity to calibrate TM data using MODISA data, making it possible to extend recent observations to the 1980s and 1990s to form a continuous time series to the present. Towards this goal, Landsat 5 TM data were first processed using customized atmospheric correction to generate surface reflectance data (described below), which were then compared to concurrent MODISA reflectance data derived using a similar atmospheric correction approach. Contingent upon agreement between the sensors, MODISA data could be "back-casted" using historical TM data.

All Landsat 5 TM band 1–7 data from 1984 to 2010 for scenes (row-path) 015–043 and 016–043 (centering on the upper and lower Florida Keys, respectively) were obtained from the U.S. Geological Survey (USGS). Images with extensive cloud cover (approximately 75%) over the study area were excluded, leaving a total of 587 images with minimal cloud cover. The digital counts data were converted to top-of-atmosphere (TOA) radiance (L_t, mW cm^{-2} μm^{-1} sr^{-1}), then binned into groups of 64 (8 × 8) in order to increase the SNR. The resulting data were thereby converted to 240 m resolution via neighborhood averaging. The maximum SNRs of these binned pixels are 8 times that of the original Landsat TM SNRs (72:1 in the blue to 29:1 in the red for typical radiances over the ocean, Hu et al., 2012), making them comparable to the SNRs of MODISA land bands. After atmospheric correction, the data were further binned to 1-km resolution, with a reduction in noise to further match the MODISA 1-km bands.

The atmospheric correction of MODISA is based on the principles and procedures detailed in Gordon and Wang (1994) and Gordon (1997), and then updated in Wang and Shi (2007). The sophisticated scheme derives the aerosol properties in the visible bands through extrapolation of the near-infrared (NIR) or shortwave-infrared (SWIR) measurements, and is embedded in the software package SeaDAS (version 6.2 and higher). To assure consistency, a procedure similar to MODISA atmospheric correction has been implemented for Landsat. Although interested readers can refer to the published literature for the theoretical basis and detailed steps, for completeness of this paper the procedure is briefly described below.

For every image pixel, after correcting the gas absorption effects (in particular, ozone and water vapor) L_t is a result of the water-leaving radiance, L_w, after propagating through the atmosphere and being superimposed on the atmospheric path radiance due to Rayleigh and aerosol scatterings (L_r and L_a):

$$L_{t,\lambda}(\Theta) = L_{r,\lambda}(\Theta) + L_{a,\lambda}(\Theta) + t_\lambda L_{w,\lambda}(\Theta), \quad (1)$$

where λ is the wavelength, Θ represents the solar-viewing geometry (solar zenith and sensor zenith angles and their relative azimuth), and t is the pixel-to-satellite diffuse transmittance at sensor zenith angle of θ. Here, for simplicity, the contributions from whitecaps and sun glint are omitted. Once $L_{w,\lambda}$ is obtained from $L_{t,\lambda}$, it is further converted to remote sensing reflectance ($R_{rs,\lambda}$, sr^{-1}) by

$$R_{RS,\lambda} = L_{w,\lambda} / \left[F_{o,\lambda} \cos_o t_{o,\lambda} \right], \quad (2)$$

where t_o is the diffuse transmittance from the sun to the pixel at the solar zenith angle of θ_o, and F_o is the extraterrestrial solar irradiance adjusted for the sun–earth distance. $R_{RS,\lambda}$ is a fundamental parameter used for nearly all remote sensing inversion algorithms to estimate water quality parameters or benthic properties, and is the ultimate goal of atmospheric correction of satellite ocean color measurements.

For every image pixel, assuming negligible L_w or R_{RS} in the SWIR Landsat TM bands at 1.6 and 2.2 μm (SWIR1 and SWIR2, respectively), L_t in these bands is a result of atmospheric scattering and can be used to derive atmospheric path radiance and diffuse transmittance in other bands. In practice, the radiative transfer simulation software package MODTRAN4 (US Air Force Research Laboratory) was first used to determine Rayleigh scattering for each image-specific Θ, surface pressure, humidity, and ozone. Ancillary data from the National Centers for Environmental Prediction, Ozone Monitoring Instrument and Total Ozone Mapping Spectrometer were obtained to ascertain air pressure, relative humidity and ozone concentration for each individual scene.

MODTRAN was then used to estimate total and Rayleigh reflectance for two extreme aerosol types (maritime and tropospheric). Aerosol reflectance for these two aerosol types (ρ_A^{Mari} and ρ_A^{Tropo}, respectively) was estimated by subtracting Rayleigh from total reflectance. SWIR band ratios [ε(λ)] were then calculated for all TM bands for both aerosol type conditions by:

$$\varepsilon_{MODTRAN}^{Mari}(\lambda, SWIR2) = \frac{\rho_A^{Mari}(\lambda)}{\rho_A^{Mari}(SWIR2)} \quad (3)$$

and

$$\varepsilon_{MODTRAN}^{Tropo}(\lambda, SWIR2) = \frac{\rho_A^{Tropo}(\lambda)}{\rho_A^{Tropo}(SWIR2)}. \quad (4)$$

The relationship between the SWIR1 band ratios from these extreme aerosol cases and that of the TM data (ε) was calculated as

$$ratio = \frac{\varepsilon(SWIR1, SWIR2) - \varepsilon_{MODTRAN}^{Mari}(SWIR1, SWIR2)}{\varepsilon_{MODTRAN}^{Tropo}(SWIR1, SWIR2) - \varepsilon_{MODTRAN}^{Mari}(SWIR1, SWIR2)}. \quad (5)$$

This ratio was used to estimate aerosol ε for the other TM bands as

$$\varepsilon(\lambda, SWIR2) = \left(\varepsilon_{MODTRAN}^{Tropo}(\lambda, SWIR2) - \varepsilon_{MODTRAN}^{Mari}(\lambda, SWIR2) \right) * ratio + \varepsilon_{MODTRAN}^{Mari}(\lambda, SWIR2). \quad (6)$$

Then, MODTRAN was used to estimate the atmospheric effects (path radiance and diffuse transmittance), finally resulting in R_{RS} for each pixel. Note that although the concept of this atmospheric correction is identical to that used for MODISA ocean color measurements, there are two differences in their implementations. The first is that the spectral slope of aerosol scattering (ε) is defined here using multiple instead of single scattering. The second is that only two aerosol types are used to bracket the aerosol reflectance. This is analogous to the atmospheric correction of the 8-bit CZCS data (Gordon & Morel, 1983). Meanwhile the use of the SWIR bands of Landsat TM will minimize the potential contamination of the water signal to the total signal, making atmospheric correction easier for coastal waters.

The TM R_{RS} data were then reprojected from their native Universal Transverse Mercator to a geographic latitude/longitude cylindrical projection whereby each pixel has 1 km resolution using bilinear interpolation. Although atmospheric correction was accomplished at 240 m resolution, 1 km resolution was used in order to reduce the image noise and to match the native resolution of the MODISA ocean color bands. Pixels with R_{RS} above 0.05 sr^{-1} in any wavelength were flagged as likely cloudy. To account for cloud shadow effects, an erosion operator was applied to these flagged TM pixels, meaning that the furthest extent of cloudy regions was widened by at least 1 km and subsequently removed from further analyses.

MODISA data from 2002 to 2010 and within the range 24° to 26° N, 80° to 83° W (a total of 2797 images) were downloaded from NASA Goddard Space Flight Center (GSFC). These data were processed using the standard atmospheric correction (SWIR and NIR combined; Wang & Shi, 2007) embedded in SeaDAS (version 6.2) to obtain R_{RS} for every MODISA band. Pixels determined to be cloudy by the CLDICE (cloud or ice detected) algorithm (Patt et al., 2003) in bit 10 of the Level-2 processing flags (i.e., Rayleigh-corrected reflectance at 869 nm > 0.027) were removed from further analysis. The resulting R_{RS} data were also reprojected to the same geographic latitude/longitude cylindrical projection at 1 km resolution so data can be compared directly with Landsat R_{RS}.

Land pixels (including a 1 km coastline) were excluded from all analyses, as were pixels outside the Florida Bay, Southwest Florida Bight and FRT regions. Image processing and analyses were performed using SeaDAS, ENVI version 4.8 (Research Systems, Inc.) and IDL version 8.0 (ITT Visual Information Systems). Statistical metrics used in this analysis and TM atmospheric correction were performed using Matlab version R2011a (MathWorks).

4. Results and discussion

4.1. Cross-sensor agreement

Concurrent (within ~3 h) and collocated MODISA and TM R_{RS} measurements, hereby called 'matchups' (n), were extracted and compared by linear regression for all three bands. Positive linear trends described the relationships between the MODISA and TM data in the blue (n = 194144; $r^2 = 0.84$; Fig. 3a), green (n = 201131; $r^2 = 0.88$; Fig. 3b), and red (n = 110626; $r^2 = 0.88$; Fig. 3c) bands. The number of pixels differs for the three different bands due to negative R_{RS}, especially in the red band.

Regardless of the high scattering, most of the data (>20 matchup data density on the color legend) are centered around the 1:1 lines for all three bands, suggesting both the success of the TM atmospheric correction and the potentials for using TM R_{RS} to extend MODIS R_{RS} to the 1980s and 1990s. Some of the large residuals, as well as discrepancies from the 1:1 line, likely resulted from the difference in spectral resolution (see Fig. 1). For example, the shortest wavelength with larger than 10% relative spectral response on the MODISA band 10 is 481 nm. In contrast, TM band 1 is largely unaffected by wavelengths less than 447 nm. Even though colored dissolved organic matter (CDOM) absorption affects R_{RS} for both of these wavebands, the effect on R_{RS} is larger in the shorter wavelengths. As the study region is typically CDOM rich, the linear regression slope of less than 1 between TM and MODISA R_{RS} matchups in the blue band is likely a result of the CDOM effect on the different bandwidths (Fig. 3a). Differences in the instrument radiometric calibrations, digitization bits (12 for MODIS, 8 for TM), and possibly SNRs, as well as insufficient cloud masking, may further explain some of the scatter in Fig. 3.

To visualize cross-sensor agreement over time, MODIS red, green, and blue R_{RS} data were averaged by month for several discrete locations (1 km pixels) throughout the study region. These data were plotted with Landsat 5 TM R_{RS} from the same locations (Fig. 4). With the exception of some obvious outliers, there was generally strong agreement over time between the two sensors. True color TM imagery and MODISA imagery both show high turbidity events concomitant with

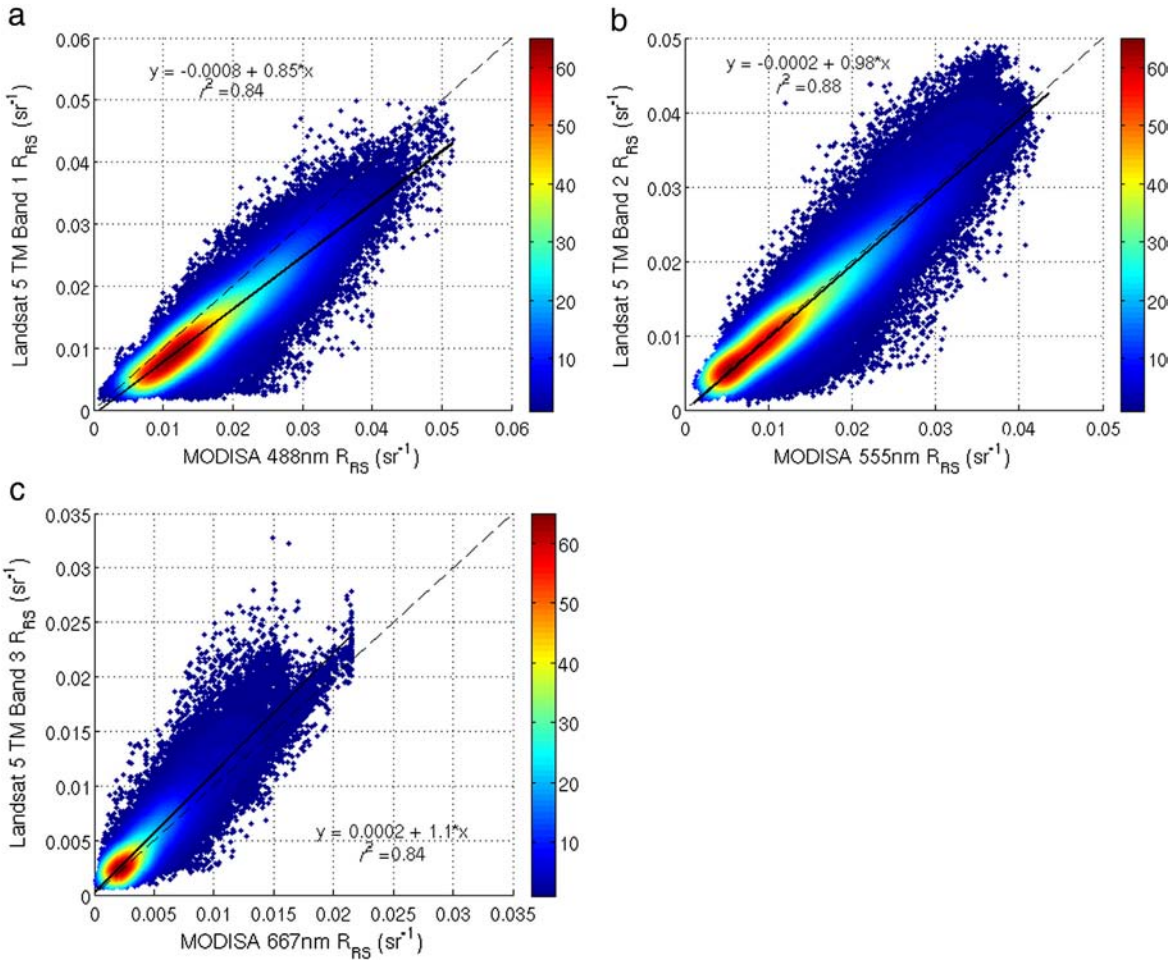

Fig. 3. Scatterplots showing matchups of MODISA and TM R_{RS} data for a) blue, b) green, and c) red bands. Color indicates density of matchups. Dotted line is the 1:1 reference while the solid black line is the linear trendline. (For interpretation of the references to color in this figure legend, the reader is referred to the web version of this article.)

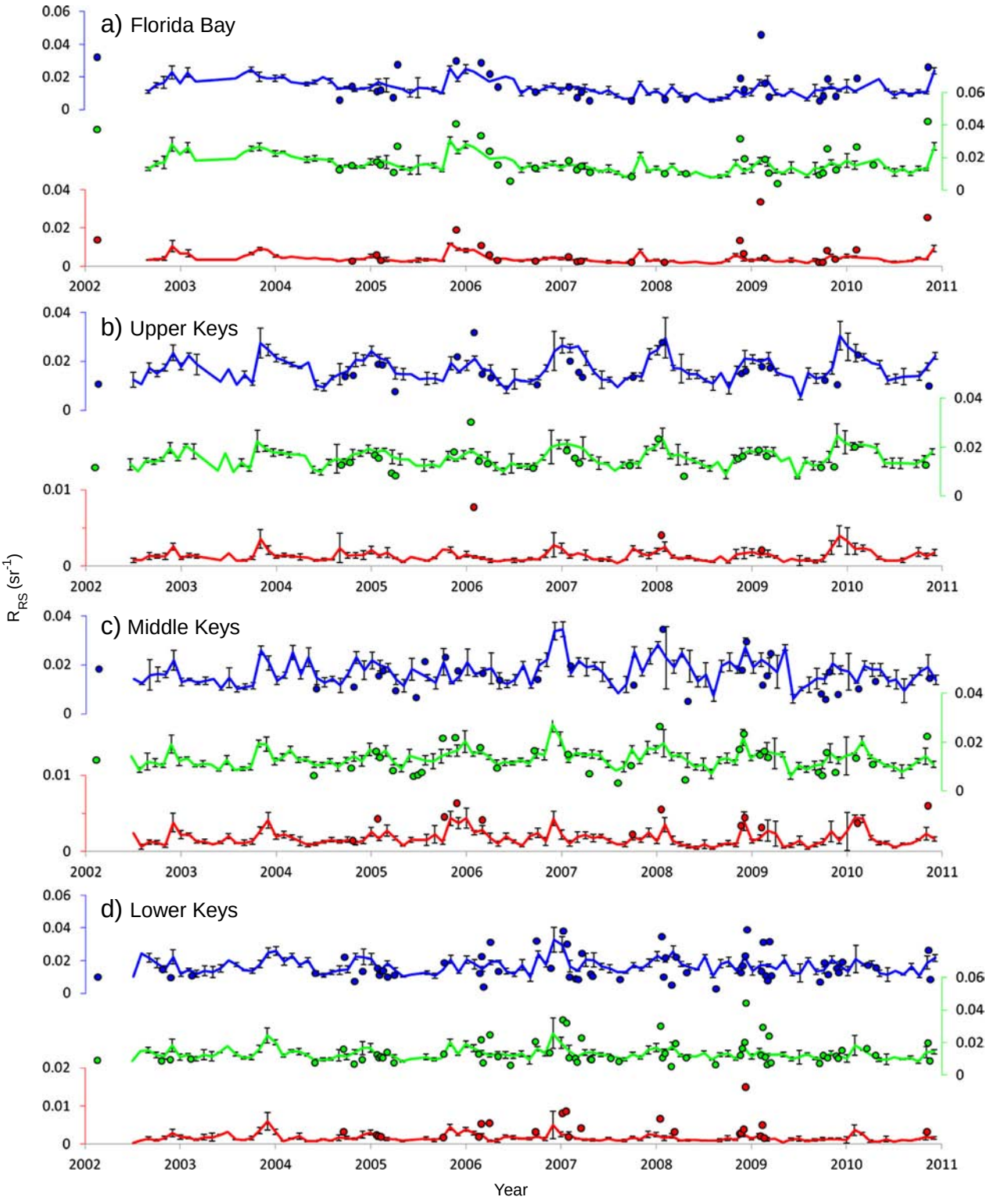

Fig. 4. Time series of red, green, and blue R_{RS} (sr^{-1}) data from TM (circles) and monthly mean MODIS (lines) for representative locations shown in Fig. 2 map for a) Florida Bay, b) Upper, c) Middle, and d) Lower Keys. Color of line indicates color of band (red, green, or blue). Error bars for MODIS data show ±1 standard error for each month. (For interpretation of the references to color in this figure legend, the reader is referred to the web version of this article.)

most of the TM outliers. In these cases, MODISA R_{RS} was also high, but not anomalous, nearby (in space and time) to the TM outliers, although this is obscured by monthly averaging in Fig. 4. Nevertheless, the relationship between TM and MODISA data appears to be consistent, with no apparent drift causing divergence of R_{RS} from the two sensors.

4.2. Anomaly detection

MODISA data were used to create band-specific monthly R_{RS} climatologies for each calendar month using data from the years 2002–2010. The mean and standard deviation of all MODISA data at

each pixel were calculated. Normalized anomalies were subsequently created for all MODISA data by subtracting the image data from its pixel-specific monthly climatological mean, then dividing by the climatological standard deviation for that pixel. TM data were also rescaled to approximate MODISA values according to the band-specific linear regression equation (Fig. 3). As with the MODISA data, normalized anomalies (relative to the MODISA climatologies) were then created for the rescaled TM data.

These continuous normalized anomaly data were then classified categorically as either positive anomaly, negative anomaly, or no anomaly in order to highlight extreme anomaly events. For MODISA data, the threshold for this distinction was +/− two standard deviations (e.g., a pixel with normalized anomaly of −2.1 was classified as negative anomaly). A stepwise (incrementally increasing by 0.1 standard deviations) approach was then taken to determine the positive and negative band-specific thresholds for categorical classification of TM anomalies based on the agreement with MODISA classifications. The final thresholds used in further analyses were the smallest (absolute) threshold with false positive rate (α) less than 0.05. This stepwise approach was necessary (as opposed to setting TM classification thresholds at +/−2 standard deviations) in order to maximize the number of true positive detections while maintaining an acceptable false positive rate. F-measures (Witten & Frank, 2005) were calculated to assess the overall classification performance. F-measures are calculated from counts of true positives (TP), false positives (FP) and false negatives (FN) as $2 * TP / (TP + FP + FN)$. Note that since the goal is to measure the correct detection of anomalies, true negatives (TN) are not included in this metric.

The blue, green, and red band thresholds for positive TM R_{RS} anomaly detection were 2.1, 1.9, and 2.3 standard deviations, while the thresholds for negative anomalies were −1.8, −1.8, −1.5 standard deviations, respectively. F-measures for the positive anomalies were 1.08, 1.18, and 1.16, respectively, indicating strong performance of the TM positive anomaly detection. F-measures for the negative anomalies were lower (0.46, 0.21, and 0.12). The low F-measures for negative anomaly detection are due, in part, to fewer numbers of MODISA negative anomalies, which are by-products from the skewness of the MODISA data (see Fig. 3). Nevertheless, all anomaly classification methods showed greater than 90% accuracy. Tables 1, 2, and 3 show confusion matrices for TM positive and negative anomaly detections in the three bands. These thresholds were applied to all MODISA and TM data in order to create categorical anomaly data for the entire time series of both instruments. Fig. 5 shows an example of categorical anomalies detected by concurrent MODISA and TM on 1 February 2005. For every band, most spatial patterns of categorical anomalies agree between MODISA and TM, further suggesting cross-sensor consistency.

Given the acceptable performance of these anomaly detection methods, categorical anomaly data were extracted from all TM categorical anomaly images along the two transects in the study region (Fig. 6). For each 1 km pixel along these transects, the TM categorical anomaly data were extracted and dummy coded (−1 for negative anomaly, 0 for no anomaly, 1 for positive anomaly). Annual averages of the dummy coded data were subsequently plotted in time series (Fig. 6).

Table 1
Confusion matrices for TM blue wavelength positive and negative R_{RS} anomaly detections.

	MODISA condition (truth)				
	Positive anomaly	No positive anomaly		Negative anomaly	No negative anomaly
TM positive anomaly	17078	8098	TM negative anomaly	3389	9283
TM no positive anomaly	6537	162431	TM no negative anomaly	1936	179536
	F-measure =	1.077		F-measure =	0.464

Table 2
Confusion matrices for TM green wavelength positive and negative R_{RS} anomaly detections.

	MODISA condition (truth)				
	Positive anomaly	No positive anomaly		Negative anomaly	No negative anomaly
TM positive anomaly	18959	7977	TM negative anomaly	1874	8064
TM no positive anomaly	5347	168849	TM no negative anomaly	1747	189446
	F-measure =	1.175		F-measure =	0.211

Table 3
Confusion matrices for TM red wavelength positive and negative R_{RS} anomaly detections.

	MODISA condition (truth)				
	Positive anomaly	No positive anomaly		Negative anomaly	No negative anomaly
TM positive anomaly	14957	3960	TM negative anomaly	362	4882
TM no positive anomaly	6824	84885	TM No negative anomaly	334	105048
	F-measure =	1.162		F-measure =	0.123

As such, a pixel which showed negative anomaly for all images within a year (minimum 3 pixels required) would have a mean anomaly of −1 (or −100%). As a result of the categorical classification and the 3 pixel per year minimum requirement, detected anomalies are only minimally affected by the sporadic outliers between MODIS and TM R_{RS} (see Section 4.1.).

The first and most important conclusion to be drawn from Fig. 6 is that instrument drift is apparently not affecting the anomaly detections presented here. Even though the TM anomaly data are based on a MODISA climatology (2002–2010), there appear to be no regular trends in the derived anomalies. As a result, oscillations through time (as are expected in natural and impacted systems) are likely the result of changing environmental parameters. Specific anomalous reflectance events must be corroborated with historical events to infer their etiology.

4.3. Anomaly interpretation

Although there are some data gaps due to lack of sufficient data in the annual averages, the long-term space-time plots of TM-derived R_{RS} anomalies between 1984 and 2010 show some coherent patterns in space and time (Fig. 6). For optically deep waters, the anomaly patterns in R_{RS} can be attributed to changes in the concentrations of water constituents. Specifically, high suspended sediment loads would be represented by positive R_{RS} anomalies in the red, green, and blue bands, while increased CDOM concentration would lower R_{RS} in the blue band (Kirk, 1994). Phytoplankton blooms would similarly lower R_{RS} in the blue band but increase R_{RS} in the green band (Kirk, 1994).

In the Florida Keys region, however, the interpretation of anomalies is not as straightforward. Many of the waters in the region could switch from optically deep to optically shallow depending on the bottom depth, bottom type, and concentrations of the water constituents. Also, the bottom type is spatially and temporally variable, which can further complicate interpretation of the R_{RS} anomalies. For instance, decreasing turbidity would cause R_{RS} in the red band to decrease until the water becomes optically shallow. Then, further decreases in turbidity for optically shallow waters could result in an apparent increase in the red band R_{RS} for a sandy (bright bottom) environment. Alternatively, a change in benthic albedo resulting from loss of seagrasses in an optically

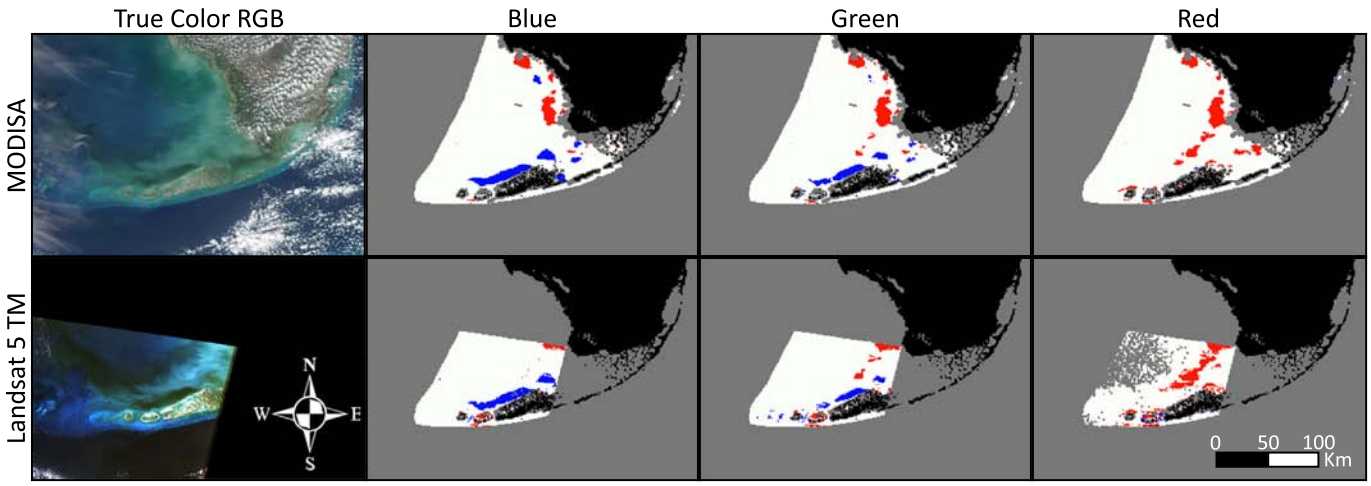

Fig. 5. MODISA (top row) and Landsat-5 TM (bottom row) RGB and R_{RS} categorical anomaly images for 1 February 2005. Pixels with positive anomalies are marked as red; negative anomalies are in blue. White pixels represent no anomaly, while gray pixels have no data (clouds) or are masked for depth. Land is shown in black.

shallow region could result in a similar (albeit likely more long term) R_{RS} increase in both the green and red bands. As a result, a single large scale change in environmental parameters may be manifested in different (or even opposing) R_{RS} signatures depending on the location or previous conditions.

Based on published literature describing the environmental changes in the study region (see Boyer & Jones, 2002; Durako, Hall, & Merello, 2002; Hall, Durako, Fourqurean, & Zieman, 1999; Hu et al., 2003, 2004; Lapointe, Bedford, & Baumberger, 2007, Lapointe et al., 2004; Prager & Halley, 1999; Robblee et al., 1991; Stumpf et al., 1999;

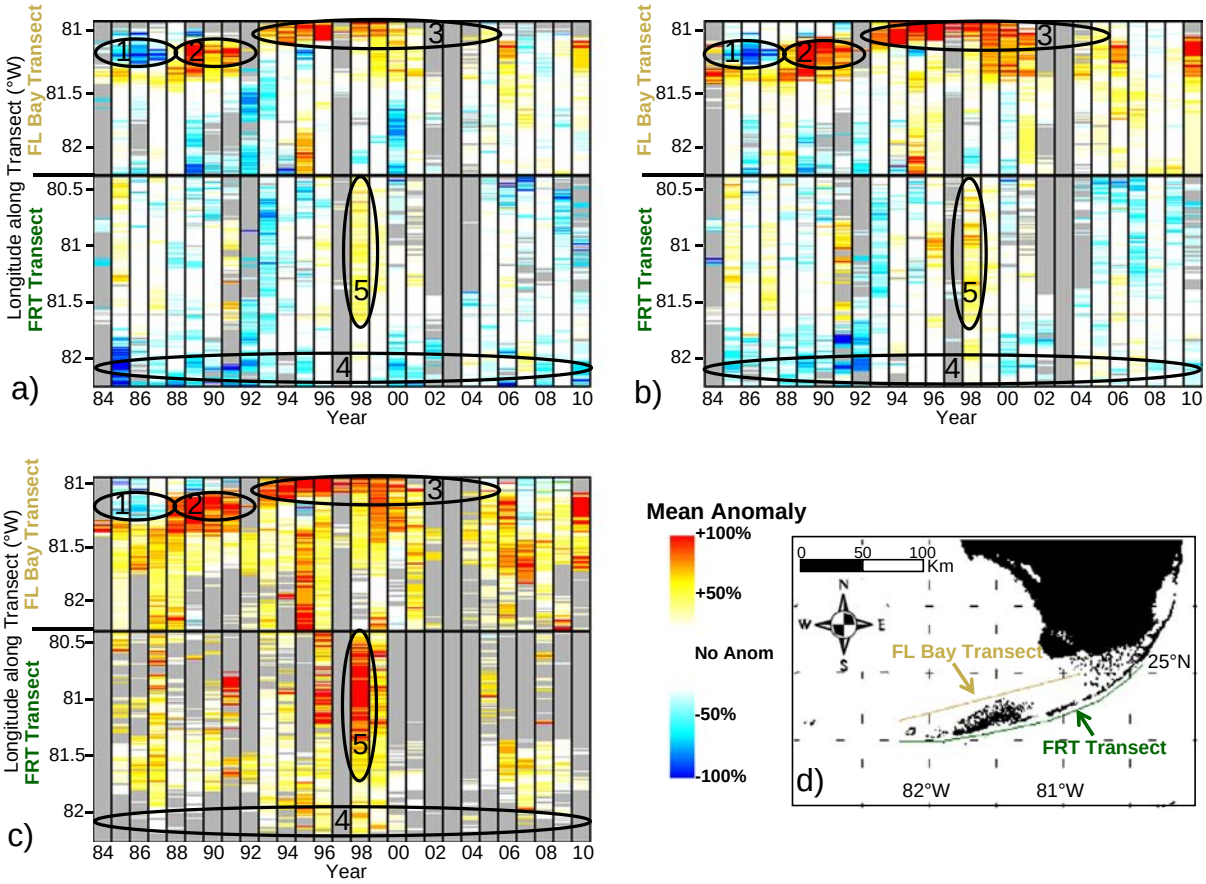

Fig. 6. Landsat TM time series of mean annual R_{RS} anomaly for a) blue, b) green, and c) red bands along the FRT transect (green line in d). Gray points represent fewer than three valid pixels for that year (x-axis) and longitude along the transect (y-axis). Mean anomaly is derived as the average of the R_{RS} categorical anomaly for a pixel (e.g., a −100% mean anomaly means that all data for that pixel in that year showed negative anomaly). Circled regions are discussed in the text.

Thayer, Murphey, & LaCroix, 1994) and on long-term river flow and wind speed data, below we attempt to interpret the R_{RS} anomaly patterns revealed by Landsat TM data in the three visible bands. Note that ideally, satellite-derived water quality parameters (water clarity or turbidity, chlorophyll-a concentration, CDOM absorption, etc.) would be used to determine the etiology of R_{RS} anomalies. However, currently there is no reliable algorithm to convert TM R_{RS} data to water quality parameters in such optically complex coastal environments. While future effort will be dedicated to such algorithm development, a qualitative interpretation of the R_{RS} anomaly patterns is provided below for the two pre-selected transects. The agreement between TM-detected R_{RS} anomalies and those predicted by known environmental changes serves as an indirect validation of the overall approach, and also sheds light on the larger spatiotemporal context of these environmental changes.

4.3.1. Florida Bay/Southwest Florida Bight

The most prominent features observed in the Florida Bay transect (Fig. 6) were anomalously high R_{RS} events on the eastern end of the transect (east of 81.5 W). From the beginning of the time series to 1987, negative anomalies were seen in all three bands to the west of Florida Bay (approximate longitude 81.25 W, Fig. 6, circle 1). In 1988, these shifted to strongly positive anomalies which diminished in intensity around 1992 (Fig. 6, circle 2). Stumpf et al. (1999) found very similar trends in the red band reflectance at the same location using AVHRR data spanning the years 1985 to 1997. Specifically, Stumpf et al. (1999) showed "low reflectance in 1986–1987, high reflectance in 1988–1991, and low to moderate reflectance after that time," noting that the recovery of reflectance was "not quite to the reflectance range observed in 1986." The change from low to high reflectance was attributed to seagrass die-offs beginning in 1987 (Robblee et al., 1991), while the subsequent return to previous R_{RS} indicated "some increase in bottom cover" (Stumpf et al., 1999). Although in situ studies (Durako et al., 2002; Hall et al., 1999; Thayer et al., 1994) have not shown such increases of the dominant seagrass species (*Thalassia testudinum*) in this region, abundance of species adapted to lower light conditions (*Halodule wrightii* and *Halophilia engelmannii*) have increased in western Florida Bay (Durako et al., 2002).

Further, Stumpf et al. (1999) noted substantial increases in the red-band reflectance within northwest Florida Bay (approximately 81 W, circle 3 in Fig. 6) starting in 1992 and continuing through the end of the study (1997). To our knowledge, the work by Stumpf et al. (1999) is the only long-term and spatially-synoptic investigation of water clarity and benthic cover in this region during the time gap without satellite ocean color coverage. The strong agreement between their results and the current study gives credence to the methodologies presented here, and justifies the wider (in space and time) interpretation of our findings. The current study expands on the results of Stumpf et al. (1999) by putting findings in a longer time context, while adding reflectance data for blue and green wavebands.

Specifically, we find that the high reflectance in northwest Florida Bay (Fig. 6, circle 3) described as increased turbidity and/or loss of seagrass by Stumpf et al. (1999) continued until at least 2001. After 2001, lack of TM data precluded continued assessment of this anomaly until 2005, at which point reflectance in northwest Florida Bay returned to previous (1984–1991) levels. Given the timing of these shifts compared to freshwater inputs to the region and the fact that these high anomalies were seen in all three TM bands, it is likely that turbidity is the main factor driving the high reflectance. Loss of seagrass cover may have exacerbated this turbidity by subjecting the benthos to greater wave energy (Prager & Halley, 1999), or may have contributed to the high R_{RS} anomalies by exposing sandy benthos.

The South Florida Water Management District (SFWMD) collects and maintains long-term datasets of daily flow rates for the Shark and Caloosahatchee Rivers (Fig. 7a). These data are continuous for both rivers from 1978 to present, and the average (1978–2010) annual combined river flow is 1.97 million acre-feet of water per year (afy). From 1984 to 1992, the mean was only 1.27 million afy. In contrast, the mean annual combined river flow from 1993–2005 was more than double (2.73 million afy) than that of the previous time span. Finally, the low flow condition was present again from 2006 to 2010, with the average annual combined river flow in this span at 1.27 million afy.

To illustrate the potential effects of these shifts in water flow regimes on the spatial extent of R_{RS} changes in the region, mean anomaly images for each of these 3 time spans were created (Fig. 7b). These images highlight major changes in R_{RS}, most notably in northwest Florida Bay (red arrows in Fig. 7b). In this region, low R_{RS} anomalies in the low flow periods are in stark contrast to widespread high anomalies in the wet period. As stated above, we find that changes in turbidity associated with these shifts in water flow regimes are likely the causative factor leading to the changes in red, green, and blue anomalies in the northwest Florida Bay.

In the western portion of the SW Florida Bight, a similar cycle of negative anomalies is seen (blue arrows in Fig. 7b), but only in the blue wavelengths. This region is relatively deep (20–30 m) and is not a seagrass habitat (see Fig. 2). The spectral composition of these anomalies is indicative of black water events which have been previously reported in the Florida Bight (Hu et al., 2003, 2004). Although the Florida Fish and Wildlife Conservation Commission regularly samples south Florida waters for the purposes of identifying and monitoring *Karenia brevis* (dinoflagellate red tide species) blooms, this region is surprisingly undersampled, and no such data were collected in this region of negative anomalies during the 1984–1992 time period. Unfortunately, in the absence of corroborating in situ data, we can only speculate on the etiology of this large region of negative anomalies during the 1984–1992 time period.

4.3.2. Florida Reef Tract

Compared to the Florida Bay transect, the R_{RS} anomalies along the FRT transect are relatively minor and transient. Along the FRT transect, one notable feature is west of 82 W (Fig. 6, circle 4), where negative anomalies in the blue and green bands were common prior to 1992 (also seen in Fig. 7b, orange arrows). This region subsequently has seen regular blue-band anomalies, with green anomalies being more infrequent (Fig. 6). Despite abundant seagrasses, this area has been reported as having the highest chlorophyll concentration (Boyer & Jones, 2002) and diffuse attenuation coefficient (Barnes et al., 2013) in the FRT region owing to nutrient inputs from Florida Bay and the SW Florida Bight. Since these anomalies are based on the mean and standard deviation climatologies at each pixel, this feature does not describe spatial differences in R_{RS} along the reef tract. Instead, this feature likely indicates a loss or thinning of seagrass coincident with the beginning of the 1992–2006 wet period. The elevated nutrient concentrations in waters advected from Florida Bay could cause epiphytization or shading by increases in phytoplankton blooms (Lapointe et al., 2004, 2007). Lack of data in the red band makes further interpretation difficult.

Positive anomalies were seen for all three TM bands along the FRT in 1998 (Fig. 6, circle 5). True color Landsat images show extreme turbidity events which covered the FRT in March, April and November 1998. SWFMD data show that combined Caloosahatchee and Shark river discharge was high in 1998 (3.3 million afy), however such positive R_{RS} anomalies and large scale extreme turbidity events were not seen in the FRT for other high flow years. Hourly wind data collected by the National Data Buoy Center (NDBC) stations in the region show above-average wind speed in the FRT preceding the turbidity events in March and April, but not in November. Nevertheless, these large scale turbidity events undoubtedly reduced the light available to benthic habitats. Such turbidity could have detrimentally impacted FRT coral environments via sedimentation (see Rogers, 1990). It is worth noting that due to extremely elevated temperatures resulting from El Niño conditions, mass bleaching of coral tissues was observed globally in summer 1998 (Hoegh-Guldberg, 1999). This mass bleaching did not contribute to the positive mean R_{RS} anomalies along the FRT transect in 1998, as

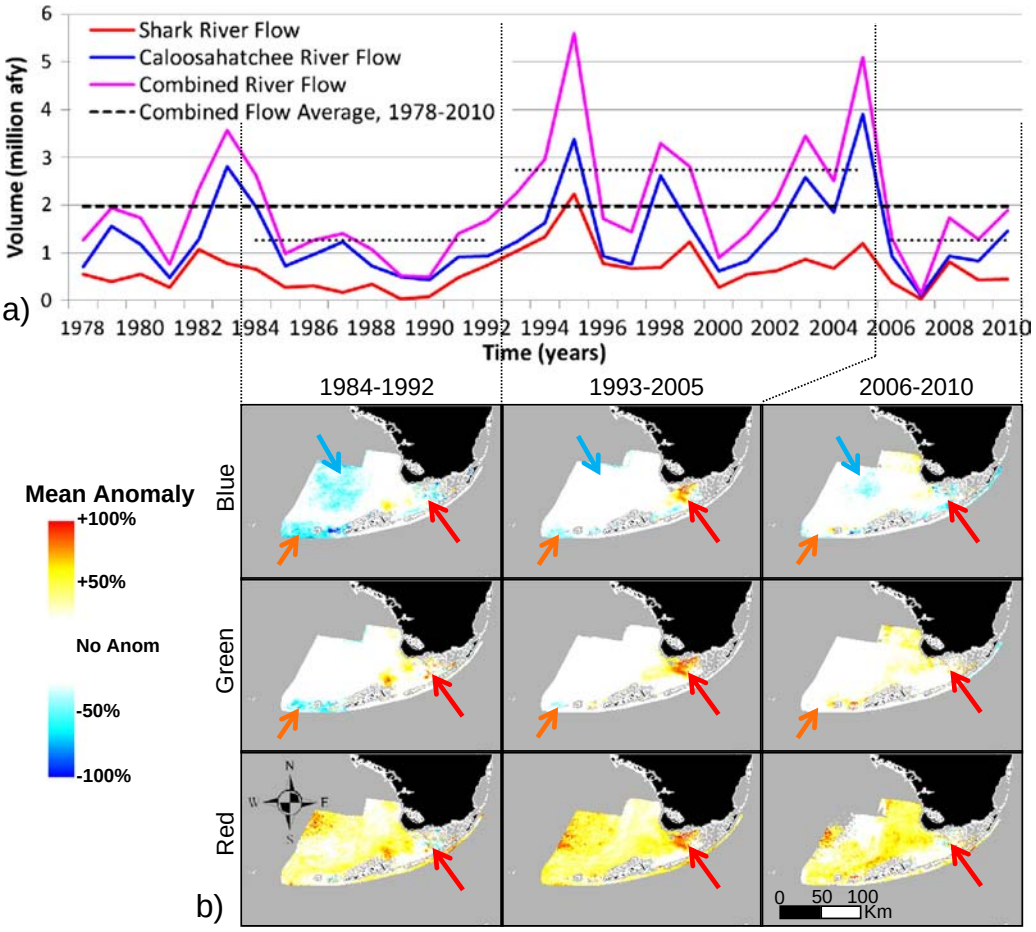

Fig. 7. a) Annual river flow of the Shark River (red) and Caloosahatchee River (blue), as well as their combined flow (purple). Horizontal lines represent mean annual combined flow for the entire time series (dashed), as well as for demarked wet and dry flow regimes (dotted). b) Average Landsat TM R_{RS} anomaly images for blue (top row), green (middle row), and red (bottom row) bands corresponding to the three demarked time periods. Arrows indicate regions where marked differences in R_{RS} anomalies were observed (see text for details).

the only summertime TM scene from 1998 did not show such positive anomalies.

Less intense, but similarly widespread R_{RS} positive mean anomalies were seen along the FRT in 1985 and 1991 (Fig. 6, not circled). For both years, TM true color images show turbidity events in the first three months of the year. Unlike the turbidity events observed in 1998, however, the turbidity in 1985 and 1991 does not visually appear to be uncharacteristic for wintertime images. Nevertheless, this analysis indicates that these events resulted in R_{RS} anomalies, indicating severity of events which is not discernible from visual interpretation of the TM imagery. Very low combined Caloosahatchee and Shark river flow was observed in both 1985 and 1991. NDBC buoy wind data coverage is extremely limited during these years, but land-based stations in Key West, FL (Key West International Airport and Key West Naval Air Station, data collected from NOAA National Climactic Data Center), showed typical wind patterns (speed and direction) in the early months of both 1985 and 1991. As demonstrated for other R_{RS} anomalies discerned from TM data in the region, such turbidity events can have detrimental effects on coral and seagrass environments (Lapointe et al., 2004; Rogers, 1990).

Palandro et al. (2001, 2008) found changes in FRT coral cover using Landsat data, corroborated by field measurements. No such shifts are seen for the FRT in the current study for several reasons. First, the 1 km spatial resolution is too large to detect benthic albedo changes on the scale of coral cover loss in the FRT. Second, TM bands were analyzed individually as opposed to being used for benthic classification of pixels. As a result, subtle shifts in R_{RS} spectra are not attributable to changes from coral to macroalgae-dominated environments.

4.4. General applications

Despite the preliminary success in establishing a MODISA-compatible Landsat TM time series for the study region, the use of Landsat data for interpretation of coastal waters and benthic environments in general requires caution. The low repeat sampling frequency can mean that large episodic events (e.g., hurricanes) may be underrepresented or missed completely. The paucity of TM data is exacerbated by clouds; the seasonality of which can result in a temporally biased dataset. For example, only two days in July 2002–2010 had both MODISA and Landsat 5 TM cloud-free data. This can have a potentially large effect on the validation of the anomaly detection methods. However, since the regression equations describing the relationship between MODISA/TM matchups did not vary greatly by month, we find application of the anomaly classification methods to be applicable to all months. Finally, the irregularity of cloud-free TM data can further affect the interpretation of the annual averages. As such, standardization of TM data to MODISA monthly reference climatologies was necessary to ameliorate this potentially confounding effect. Nevertheless, we have focused our interpretation of trends and events on anomalies that persist over many years or wide spatial scales, having been present in numerous satellite measurements. The resulting lack of temporal resolution for investigation of R_{RS} anomalies is

offset by the increased confidence in the presence of noted events and trends.

Both MODISA and Landsat TM have global coverage. Thus, it is possible to extend the approach detailed here to other coastal regions in the world. This is because MODISA atmospherically corrected R_{rs} data are readily available from NASA, and with little effort the MODTRAN-based atmospheric correction can be applied to Landsat data from USGS. This may greatly facilitate studies to track water quality events in the 1980s and 1990s. In our study region, we found long term in situ datasets to be helpful in interpreting some of the observed R_{RS} anomalies, highlighting the importance of regular in situ environmental monitoring. However, such extraneous data are by no means required to conduct similar analyses of R_{RS} anomalies elsewhere. Indeed, the deciphering of TM R_{RS} anomalies with known water quality and benthic ecosystem changes was demonstrated here as an indirect validation of the methodology. We found that visual interpretation of the Landsat images, although useful in explaining observed R_{RS} anomalies, was in itself insufficient to detect certain events (e.g., seagrass density or composition changes), or to place events in the context of climatological norms (e.g., turbidity events). For example, in some cases, R_{RS} anomalies in the FRT were clearly attributable to turbidity events (i.e., visible in TM imagery). However, as similar turbidity events are also visible in TM imagery in years when no R_{RS} anomalies were detected, this approach allowed for explication of the severity of such events, and thus their potential impact on the environment.

At the time of this writing, Landsat 5 has stopped functioning and Landsat 7 has missing data due to the SLC error. However, with an additional blue band, Landsat 8 began normal operations on 30 May 2013. The immediate next step is then to validate the consistency between Landsat 8 and MODISA during their overlapping period (i.e., after May 2013) so that Landsat 8 can provide continuous water quality observations in case the already 12-year old MODISA malfunctions.

5. Conclusions

The Landsat dataset presented here precedes the first reported major benthic environment shifts in the Florida Keys region, and provides a continuous 25 year record from which to analyze the spatial and temporal scales of these changes. In contrast to AVHRR data (see Stumpf et al., 1999), Landsat bands across the visible spectrum can be used to identify the specific etiology of R_{RS} anomaly events. As such, several large R_{RS} anomaly events, as measured by Landsat TM in the Florida Bay, have been identified and corroborated by previously documented events, including seagrass loss and turbidity increases. Many of the anomalies in Florida Bay R_{RS} coincide with periods of disparate water flow regimes from the Shark and Caloosahatchee Rivers.

This analysis indicates that large effects of freshwater flows in the Florida Bay are greatly muted in the FRT region. Although the linkage between Everglades discharge and nutrient enrichment of the FRT region has been established (Lapointe et al., 2002, 2004, 2007), it is likely that the yearly averaging has obscured this connection. Indeed, primarily transient changes in yearly-averaged R_{RS} anomalies were noted south of the Florida Keys. However, previously unreported declines in seagrasses in the Marquesas Keys region appear to also coincide with the major increase in water flow to Florida Bay, and large turbidity events in 1998 appear to result primarily from high winds and riverine discharge.

Overall, this work highlights the need for wider spatial and temporal assessment of ecosystem changes, including water quality fluctuations as well as variations in coral health and seagrass density. Such changes in the environments of the Florida Keys appear to be significantly impacted by agriculture and management within the Everglades region. The impacts of proposed resource management actions must be better understood as they pertain to nutrient enrichment, hypersalinity, and the health of the downstream Florida Keys ecosystems. Likewise, the availability of global Landsat data, in combination with this newly proposed approach to assure multi-decadal data consistency, may greatly facilitate synoptic assessment of the coastal environments for much longer periods than enabled by modern satellite sensors starting from the late 1990s.

6. Acknowledgments

This work was supported by the U.S. National Aeronautics and Space Administration through its Decision Support program, Gulf of Mexico program, Ocean Biology and Biogeochemistry program, and Water and Energy Cycle program. Relative spectral response functions of Landsat TM and MODIS were provided by NASA. Shapefiles for seagrass and coral reef locations were provided by Florida Fish and Wildlife Research Institute. Landsat data and raster bathymetry were provided by the USGS. The authors wish to thank two anonymous reviewers whose critiques greatly improved this manuscript.

Reference

Ahlnäs, K., Royer, T. C., & George, T. H. (1987). Multiple dipole eddies in the Alaska Coastal Current detected with landsat thematic mapper data. *Journal of Geophysical Research, 92*, 13041–13047.

Ault, J. S., Bohnsack, J. A., Smith, S. G., & Luo, J. (2005). Towards sustainable multispecies fisheries in the Florida, USA, coral reef ecosystem. *Bulletin of Marine Science, 76*, 595–622.

Barnes, B. B., Hu, C., Schaeffer, B.A., Lee, Z., Palandro, D. A., & Lehrter, J. C. (2013). MODIS-derived spatiotemporal water clarity patterns in optically shallow Florida Keys waters: A new approach to remove bottom contamination. *Remote Sensing of Environment, 134*, 377–391.

Boyer, J. N., & Jones, R. D. (2002). A view from the bridge: External and internal forces affecting the ambient water quality of the Florida Keys National Marine Sanctuary (FKNMS). In J. W. Porter, & K. G. Porter (Eds.), *The Everglades, Florida Bay, and coral reefs of the Florida Keys: An ecosystem source book* (pp. 609–628). Boca Raton, FL: CRC Press.

Bureau, U.S.C. (2011). *Census 2010 summary file 1, Florida.* U.S. Census Bureau.

Causey, B.D. (2002). The role of the Florida Keys National Marine Sanctuary in the south Florida ecosystem restoration initiative. In J. W. Porter, & K. G. Porter (Eds.), *The Everglades, Florida Bay, and coral reefs of the Florida Keys, an ecosystem source book* (pp. 883–894). Boca Raton, FL: CRC Press.

Dekker, A. G., & Peters, S. W. M. (1993). The use of the Thematic Mapper for the analysis of eutrophic lakes — A case study in the Netherlands. *International Journal of Remote Sensing, 14*, 799–821.

Durako, M. J., Hall, M.O., & Merello, M. (2002). Patterns of change in the seagrass dominated Florida Bay hydroscape. In J. W. Porter, & K. G. Porter (Eds.), *The Everglades, Florida Bay, and coral reefs of the Florida Keys, an ecosystem source book* (pp. 523–538). Boca Raton, FL: CRC Press.

Dustan, P. (2003). Ecological perspectives: The decline of Carysfort Reef, Key Largo, Florida 1975–2000. *Ecological forecasting: New tools for coastal and marine ecosystem management, NOAA Technical Memorandum NOS NCCOS, 1*, 37–43.

Ebersole, J. P. (2001). Recovery of fish assemblages from ship groundings on coral reefs in the Florida Keys National Marine Sanctuary. *Bulletin of Marine Science, 69*, 655–671.

Ekstrand, S. (1992). Landsat TM based quantification of chlorophyll-a during algae blooms in coastal waters. *International Journal of Remote Sensing, 13*, 1913–1926.

Fourqurean, J. W., & Robblee, M. B. (1999). Florida Bay: A history of recent ecological changes. *Estuaries, 22*, 345–357.

Franz, B. (2003). *A long-term intercomparison of oceanic optical property retrievals from MODIS-Terra and SeaWiFS.* MODIS validation, data merger, and other activities accomplished by SIMBIOS project: 2002–2003. Greenbelt, MD: NASA Goddard Space Flight Center.

Franz, B.A., Kwiatkowska, E. J., Meister, G., & McClain, C. R. (2008). Moderate resolution imaging spectroradiometer on Terra: Limitations for ocean color applications. *Journal of Applied Remote Sensing, 2*, 023525.

Garrison, V. H., Shinn, E. A., Foreman, W. T., Griffin, D. W., Holmes, C. W., Kellogg, C. A., et al. (2003). African and Asian dust: From desert soils to coral reefs. *BioScience, 53*, 469–480.

Giardino, C., Pepe, M., Brivio, P. A., Ghezzi, P., & Zilioli, E. (2001). Detecting chlorophyll, Secchi disk depth and surface temperature in a sub-alpine lake using Landsat imagery. *Science of the Total Environment, 268*, 19–29.

Gordon, H. R. (1997). Atmospheric correction of ocean color imagery in the Earth observing system era. *Journal of Geophysical Research, 102*, 17081–17106.

Gordon, H. R., & Morel, A. Y. (1983). *Remote assessment of ocean color for interpretation of satellite visible imagery.* A Review. Berlin Heidelberg, New York: Springer-Verlag (114 pp., Tokyo).

Gordon, H. R., & Wang, M. (1994). Retrieval of water-leaving radiance and aerosol optical thickness over the oceans with SeaWiFS: A preliminary algorithm. *Applied Optics, 33*, 443–452.

Hall, M., Durako, M., Fourqurean, J., & Zieman, J. (1999). Decadal changes in seagrass distribution and abundance in Florida Bay. *Estuaries, 22*, 445–459.

Hoegh-Guldberg, O. (1999). Climate change, coral bleaching and the future of the world's coral reef. *Marine and Freshwater Research, 50*, 839–866.

Hu, C. (2009). A novel ocean color index to detect floating algae in the global oceans. *Remote Sensing of Environment, 113*, 2118–2129.

Hu, C., Feng, L., Lee, Z., Davis, C. O., Mannino, A., McClain, C. R., et al. (2012). Dynamic range and sensitivity requirements of satellite ocean color sensors: Learning from the past. *Applied Optics, 51*, 6045–6062.

Hu, C., Hackett, K. E., Callahan, M. K., Andréfouët, S., Wheaton, J. L., Porter, J. W., et al. (2003). The 2002 ocean color anomaly in the Florida Bight: A cause of local coral reef decline? *Geophysical Research Letters, 30*, 1151. http://dx.doi.org/10.1029/2002GL016479.

Hu, C., Muller-Kager, F. E., Vargo, G. A., Neely, M. B., & Johns, E. (2004). Linkages between coastal runoff and the Florida Keys ecosystem: A study of a dark plume event. *Geophysical Research Letters, 31*. http://dx.doi.org/10.1029/2004GL020382 (L15307).

Jaap, W. C. (1985). An epidemic zooxanthellae expulsion during 1983 in the lower Florida Keys coral reefs: Hyperthermic etiology. *Proc. 5th Int. Coral Reef Congr., Tahiti, 6.* (pp. 143–148).

Kirk, J. T. O. (1994). *Light and photosynthesis in aquatic ecosystems.* Cambridge England; New York, NY, USA: Cambridge University Press.

Kwiatkowska, E. J. (2003). *Comparisons of daily global ocean color data sets: MODIS-Terra/Aqua and SeaWiFS.* MODIS validation, data merger, and other activities accomplished by SIMBIOS project: 2002–2003. Greenbelt, MD: NASA Goddard Space Flight Center.

Lapointe, B. E., & Barile, P. J. (2004). Comment on J. C. Zieman, J. W. Fourqurean, and T. A. Frankovich. 1999. Seagrass die-off in Florida Bay: Long-term trends in abundance and growth of turtle grass, *Thalassia testudinum. Estuaries, 22*, 460–470 (Estuaries, 27, 157–164).

Lapointe, B. E., Barile, P. J., & Matzie, W. R. (2004). Anthropogenic nutrient enrichment of seagrass and coral reef communities in the Lower Florida Keys: Discrimination of local versus regional nitrogen sources. *Journal of Experimental Marine Biology and Ecology, 308*, 23–58.

Lapointe, B. E., Bedford, B., & Baumberger, R. (2007). Looe Key, FL: Nutrients and climate change pose threat to coral reefs. In S. Bricker, B. J. Longstaff, W. C. Dennison, A.B. Jones, K. Boicourt, E. C. Wicks, & J. L. Woerner (Eds.), *Effects of nutrient enrichment in the nation's estuaries: A decade of change* (pp. 104–105). Silver Spring, MD: National Centers for Coastal Ocean Science.

Lapointe, B., & Clark, M. (1992). Nutrient inputs from the watershed and coastal eutrophication in the Florida Keys. *Estuaries and Coasts, 15*, 465–476.

Lapointe, B., Matzie, W. R., & Barile, P. J. (2002). Biotic phase-shifts in Florida Bay and fore reef communities of the Florida Keys: Linkages with historical freshwater flows and nitrogen loading from everglades runoff. In J. W. Porter, & K. G. Porter (Eds.), *Everglades, Florida Bay, and coral reefs of the Florida Keys: An ecosystem sourcebook* (pp. 629–648). Boca Raton, FL: CRC Press.

Lapointe, B., Matzie, W. R., & Clark, M. W. (1993). Phosphorus inputs and eutrophication on the Florida reef tract. In R. N. Ginsberg (Ed.), *Global Aspects of Coral Reefs* (pp. v15–v21). University of Miami: Rosenstel School of Marine and Atmospheric Science.

Lessios, H. A., Robertson, D. R., & Cubit, J.D. (1984). Spread of diadema mass mortality through the caribbean. *Science, 226*, 335–337.

Lirman, D., Schopmeyer, S., Manzello, D., Gramer, L. J., Precht, W. F., Muller-Karger, F., et al. (2011). Severe 2010 cold-water event caused unprecedented mortality to corals of the Florida reef tract and reversed previous survivorship patterns. *PLoS ONE, 6*, e23047.

Maritorena, S., & Siegel, D. A. (2005). Consistent merging of satellite ocean color data sets using a bio-optical model. *Remote Sensing of Environment, 94*, 429–440.

Miller, M. W., & Hay, M. E. (1998). Effects of fish predation and seaweed competition on the survival and growth of corals. *Oecologia, 113*, 231–238.

National Research Council (2002). *Florida Bay research programs and their relation to the comprehensive Everglades restoration plan.* Washington, D.C.: National Academies Press (54 pp.).

Olmanson, L. G., Bauer, M. E., & Brezonik, P. L. (2008). A 20-year Landsat water clarity census of Minnesota's 10,000 lakes. *Remote Sensing of Environment, 112*, 4086–4097.

Palandro, D. A., Andrefouet, S., Hu, C., Hallock, P., Muller-Karger, F. E., Dustan, P., et al. (2008). Quantification of two decades of shallow-water coral reef habitat decline in the Florida Keys National Marine Sanctuary using Landsat data (1984–2002). *Remote Sensing of Environment, 112*, 3388–3399.

Palandro, D., Andrefouet, S., Muller-Karger, F. E., & Dustan, P. (2001). Coral reef change detection using Landsats 5 and 7: A case study using Carysfort Reef in the Florida Keys. *Geoscience and remote sensing symposium, 2001. IGARSS '01. IEEE 2001 international, Vol. 622.* (pp. 625–627).

Patt, F. S., Barnes, R. A., Eplee, R. E., Jr., Franz, B.A., Robinson, W. D., Feldman, G. C., et al. (2003). Algorithm updates for the fourth SeaWiFS data reprocessing. In J. A. Yoder, S. B. Hooker, & E. R. Firestone (Eds.), *NASA technical memorandum* (2003–206892).

Phlips, E. J., Lynch, T. C., & Badylak, S. (1995). Chlorophyll a, tripton, color, and light availability in a shallow tropical inner-shelf lagoon, Florida Bay, USA. *Marine Ecology Progress Series, 127*, 223–234.

Porter, J. W., Dustan, P., Jaap, W. C., Patterson, K. L., Kosmynin, V., Meier, O. W., et al. (2001). Patterns of spread of coral disease in the Florida Keys. *Hydrobiologia, 460*, 1–24.

Porter, J. W., Kosmynin, V., Patterson, K. L., Porter, K. G., Jaap, W. C., Wheaton, J., et al. (2002). Detection of coral reef change by the Florida Keys coral reef monitoring project. In J. W. Porter, & K. G. Porter (Eds.), *The Everglades, Florida Bay, and coral reefs of the Florida Keys: An ecosystem sourcebook* (pp. 449–769). Boca Raton, FL: CRC Press.

Prager, E. J., & Halley, R. B. (1999). The Influence of seagrass on shell layers and Florida Bay mudbanks. *Journal of Coastal Research, 15*, 1151–1162.

Robblee, M. B., Barber, T. R., Carlson, P. R., Durako, M. J., Fourqurean, J. W., Muehlstein, L. K., et al. (1991). Mass mortality of the tropical seagrass *Thalassia testudinum* in Florida Bay (USA). *Marine Ecology-Progress Series, 71*, 297–299.

Rogers, C. S. (1990). Responses of coral reefs and reef organisms to sedimentation. *Marine Evology Progress Series, 62*, 185–202.

Shinn, E. A., Smith, G. W., Prospero, J. M., Betzer, P., Hayes, M. L., Garrison, V., et al. (2000). African dust and the demise of Caribbean coral reefs. *Geophysical Research Letters, 27*, 3029–3032.

Smith, N.P., & Pitts, P. A. (2002). Regional-scale and long term transport patterns in the Florida Keys. In J. W. Porter, & K. G. Porter (Eds.), *The Everglades, Florida Bay, and coral reefs of the Florida Keys: An ecosystem sourcebook* (pp. 343–360). Boca Raton, FL: CRC Press.

Stumpf, R. P., Frayer, M. L., Durako, M. J., & Brock, J. C. (1999). Variations in water clarity and bottom albedo in Florida Bay from 1985 to 1997. *Estuaries, 22*, 431–444.

Teillet, P.M., Barker, J. L., Markham, B.L., Irish, R. R., Fedosejevs, G., & Storey, J. C. (2001). Radiometric cross-calibration of the Landsat-7 ETM+ and Landsat-5 TM sensors based on tandem data sets. *Remote Sensing of Environment, 78*, 39–54.

Thayer, G. W., Murphey, P. L., & LaCroix, M. W. (1994). Responses of plant communities in Western Florida Bay to the die-off of seagrasses. *Bulletin of Marine Science, 54*, 718–726.

Thomas, A., Byrne, D., & Weatherbee, R. (2002). Coastal sea surface temperature variability from Landsat infrared data. *Remote Sensing of Environment, 81*, 262–272.

Vincent, R. K., Qin, X., Michael, R., McKay, L., Miner, J., Czajkowski, K., et al. (2004). Phycocyanin detection from LANDSAT TM data from mapping cyanobacterial blooms in Lake Erie. *Remote Sensing of Environment, 89*, 381–392.

Wang, M., & Shi, W. (2007). The NIR-SWIR combined atmospheric correction approach for MODIS ocean color data processing. *Optics Express, 15*, 15722–15733.

Wang, Y., Xia, H., Fu, J., & Sheng, G. (2004). Water quality change in reservoirs of Shenzhen, China: Detection using LANDSAT/TM data. *Science of the Total Environment, 328*, 195–206.

Warner, M. E., Fitt, W. K., & Schmidt, G. W. (1999). Damage to photosystem II in symbiotic dinoflagellates: A determinant of coral bleaching. *Proceedings of the National Academy of Sciences, 96*, 8007–8012.

Witten, I., & Frank, E. (2005). *Data mining: Practical machine learning tools and techniques.* San Francisco: Morgan Kaufmann.

Zhao, J., Hu, C., Lapointe, B., Melo, N., Johns, E. M., & Smith, R. H. (2013). Satellite-observed black water events off Southwest Florida: Implications for coral reef health in the Florida Keys National Marine Sanctuary. *Remote Sensing, 5*, 415–431. http://dx.doi.org/10.3390/rs510415.

Zieman, J. C., Fourqurean, J. W., & Frankovich, T. A. (1999). Seagrass die-off in Florida Bay: Long-term trends in abundance and growth of turtle grass, *Thalassia testudinum. Estuaries, 22*, 460–470.